Icarus 217 (2012) 740–751

Contents lists available at SciVerse ScienceDirect

Icarus

journal homepage: www.elsevier.com/locate/icarus

Vertical profiling of SO_2 and SO above Venus' clouds by SPICAV/SOIR solar occultations

Denis A. Belyaev [a,b,*], Franck Montmessin [a], Jean-Loup Bertaux [a], Arnaud Mahieux [c], Anna A. Fedorova [b], Oleg I. Korablev [b], Emmanuel Marcq [a], Yuk L. Yung [d], Xi Zhang [d]

[a] LATMOS, CNRS/INSU/IPSL, Quartier des Garennes, 11 bd. d'Alembert, 78280 Guyancourt, France
[b] Space Research Institute (IKI), 84/32 Profsoyuznaya Str., 117997 Moscow, Russia
[c] Belgian Institute for Space Aeronomy, 3 Av. Circulaire, B-1180 Brussels, Belgium
[d] Division of Geological and Planetary Sciences, California Institute of Technology, Pasadena, CA 91125, USA

ARTICLE INFO

Article history:
Available online 5 October 2011

Keywords:
Venus
Venus, Atmosphere
Spectroscopy
Photochemistry

ABSTRACT

New measurements of sulfur dioxide (SO_2) and monoxide (SO) in the atmosphere of Venus by SPICAV/SOIR instrument onboard Venus Express orbiter provide ample statistics to study the behavior of these gases above Venus' clouds. The instrument (a set of three spectrometers) is capable to sound atmospheric structure above the clouds in several observation modes (nadir, solar and stellar occultations) either in the UV or in the near IR spectral ranges. We present the results from solar occultations in the absorption ranges of SO_2 (190–230 nm, and at 4 μm) and SO (190–230 nm). The dioxide was detected by the SOIR spectrometer at the altitudes of 65–80 km in the IR and by the SPICAV spectrometer at 85–105 km in the UV. The monoxide's absorption was measured only by SPICAV at 85–105 km. We analyzed 39 sessions of solar occultation, where boresights of both spectrometers are oriented identically, to provide complete vertical profiling of SO_2 of the Venus' mesosphere (65–105 km). Here we report the first firm detection and measurements of two SO_2 layers. In the lower layer SO_2 mixing ratio is within 0.02–0.5 ppmv. The upper layer, also conceivable from microwave measurements by Sandor et al. (Sandor, B.J., Todd Clancy, R., Moriarty-Schieven, G., Mills, F.P. [2010]. Icarus 208, 49–60) is characterized by SO_2 increasing with the altitude from 0.05 to 2 ppmv, and the $[SO_2]/[SO]$ ratio varying from 1 to 5. The presence of the high-altitude SO_x species could be explained by H_2SO_4 photodissociation under somewhat warmer temperature conditions in Venus mesosphere. At 90–100 km the content of the sulfur dioxide correlates with temperature increasing from 0.1 ppmv at 165–170 K to 0.5–1 ppmv at 190–192 K. It supports the hypothesis of SO_2 production by the evaporation of H_2SO_4 from droplets and its subsequent photolysis at around 100 km.

1. Introduction

Sulfur compounds are key components of Venus' atmosphere because the planet is totally covered by H_2SO_4 droplets clouds at altitudes 50–70 km. Any significant change in the SO_x oxides above and within the clouds affects the photochemistry in the mesosphere (Esposito et al., 1997). Moreover, it may be an indicator of geological activity on the planet: a single volcanic event could disturb the atmospheric circulation and increase the delivery of SO_x to the cloud top. Sulfur oxides actively participate in the photochemistry around Venus' clouds (Mills et al., 2007). SO_2 photodissociates under the effect of the solar radiation and, reversely, is formed by SO oxidation; further oxidation leads to SO_3 formation. Finally, in combination with H_2O it gives concentrated liquid sulfuric acid (~75% H_2SO_4).

The sulfur dioxide in the venusian atmosphere was first detected from Earth-based ultraviolet observations with a mixing ratio 0.02–0.5 ppm at the cloud top (Barker, 1979). Space-based identifications of SO_2 UV absorption followed soon from Pioneer Venus orbiter (PV) and International Ultraviolet Explorer (IUE). Continuous observations from the PV in 1978–1986 showed a steady decline of the cloud top SO_2 content from ~500 ppb down to 20–50 ppb about 2 years later (Esposito et al., 1988). The gas was detected in the 200–220 nm spectral range, where the absorption cross-sections of sulfur monoxide are even larger than those of the dioxide (Fig. 1). Later, on the basis of 1978–1988 IUE data Na et al. (1990) showed that SO_2 retrieval together with SO provided better fit than without SO. The SO mixing ratio was derived as 20 ± 10 ppb with $SO_2/SO \sim 10$ at the cloud top. In 1978–1991 UV rocket soundings gave average values of 80 ± 40 ppb for the

* Corresponding author at: LATMOS, CNRS/INSU/IPSL, Quartier des Garennes, 11 bd. d'Alembert, 78280 Guyancourt, France.
E-mail address: Denis.Belyaev@latmos.ipsl.fr (D.A. Belyaev).

0019-1035/$ - see front matter © 2011 Elsevier Inc. All rights reserved.
doi:10.1016/j.icarus.2011.09.025

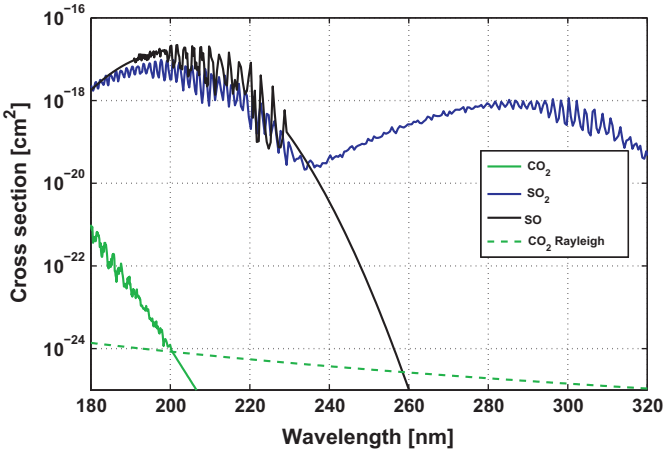

Fig. 1. Cross sections of molecular absorption and scattering (Rayleigh) that are taken into account in the UV range: CO_2 (solid green), SO_2 (solid blue), SO (solid black), Rayleigh scattering (dashed green). (For interpretation of the references to color in this figure legend, the reader is referred to the web version of this article.)

dioxide and 12 ± 5 ppb for the monoxide, in good agreement with PV and IUE simultaneous observations (McClintock et al., 1994; Na et al., 1994). One more UV measurement was done in 1995 from the Hubble Space Telescope (HST) (Na and Esposito, 1995). They found the SO_2 abundance of 20 ± 10 ppb, which was lower than values obtained in 1978–1991 by a factor of 2–5, confirming again the decrease of SO_2.

The sulfur dioxide was also measured in the infrared spectral range by the Fourier Spectrometer onboard the Venera-15 orbiter. A strong dependence of the SO_2 content on latitude at the cloud top was reported: from 20 ppb in the equator to 0.5 ppm in the polar region (Zasova et al., 1993). These data were found consistent with PV and IUE results, taking into account different effective sounding altitudes.

Recently SO_x above Venus' clouds were measured in sub-mm range from JCMT telescope in 2004–2008 (Sandor et al., 2010). The profiles of measured lines are consistent with two layers of sulfur oxides in the Venus mesosphere: <10 ppb at 70–85 km; ~30 ppb of SO and ~70 ppb of SO_2 at 85–100 km. The first retrievals of SO_2 vertical profiles from the Venus Express (VEX) mission (Titov et al., 2006) were reported from solar occultations in the IR range (SOIR) (Belyaev et al., 2008). Mixing ratios around ~0.1 ppmv at high latitudes and ~1 ppmv at low latitudes were reported at 70 km with a fast decrease to an upper limit ~0.05 ppmv at 75–80 km. This latitudinal behavior is contradicts the Venera-15 results, but is confirmed by recent SPICAV-UV observations in nadir (Marcq et al., 2011a). On the average, the SO_2 content measured by SOIR at planetary terminator occurred to be higher than previous (1987–1995) results obtained mainly on the dayside in nadir viewing. SOIR's values are also confirmed by long-slit high-resolution spectrography CSHELL from the Earth, resulted in the mean SO_2 mixing ratio of 0.35 ± 0.05 ppm near 72 km (Krasnopolsky, 2010).

In the present work, we describe a new set of SO_2 and SO measurements by SPICAV and SOIR from the VEX orbiter with some update of the previous SOIR results and first SO_x observations by SPICAV in the UV range. SPICAV-UV is sensitive to sulfur oxides' absorption band at 190–230 nm and in solar occultation probes the altitudes 85–110 km. In the occultation mode the line-of-sights (LOS) of SPICAV and SOIR spectrometers are parallel allowing simultaneous measurements. Using these data we acquired vertical profiling of SO and SO_2 in Venus' mesosphere and compared it with recent observations and modeling.

2. Observations

The SPICAV instrument – Spectroscopy for Investigation of Characteristics of the Atmosphere of Venus (Bertaux et al., 2007a) – onboard Venus Express consists of three spectrometers: SPICAV UV and IR, and SOIR. For our study we use two of them: SPICAV-UV and SOIR. In the solar occultation mode they both operate simultaneously, sounding approximately the same target altitudes. At present, 39 sessions are available for SO_x analysis located mostly around the North Pole, and a few occultations in the equatorial region (Table 1). Solar eclipses from the VEX orbit occur at ~6:00 or 18:00 of the Venus local time (except very close to the North Pole) and we probe the twilight mesosphere. SO retrievals were performed from the SPICAV-UV observations together with SO_2 while SOIR is not able to detect the SO absorption. In the selected set of sessions the earliest one was on March 28, 2007 (orbit 341) and the latest one was on October 1, 2008 (orbit 894). It gave us the possibility to monitor the evolution of sulfur oxides' content during 1.5 years (2007–2008).

In the occultation mode the instrument registers the solar flux out of planetary atmosphere and later the flux, having passed through the different levels of the atmosphere. The ratio of the second flux to the first one determines the atmospheric transmission at fixed target altitude. This transmission (a relative quantity) is interpreted as due to the extinction from aerosols and gases, which can be identified by their spectral signature, and their quantity along the LOS determined. In this sense the occultation method

Table 1
List of joint SPICAV/SOIR occultations for SO_2 detection and associated parameters. The distance to the limb defines the vertical resolution.

Orbit #	Obs. #	Date	Latitude (°)	Loc. time (h)	Dist. to limb (km)
341	18	28/03/2007	82.3	17.3	3543
356	10	12/04/2007	84.1	07.4	3475
361	18	17/04/2007	79.1	06.8	3686
366	18	22/04/2007	71.5	06.5	4163
434	1	29/06/2007	29.2	18.0	5501
435	1	30/06/2007	72.3	18.1	2184
437	9	02/07/2007	74.9	18.2	2053
441	9	06/07/2007	78.5	18.3	1939
443	8	08/07/2007	79.9	18.4	1910
447	8	12/07/2007	82.2	18.7	1886
449	4	14/07/2007	83.3	18.9	1883
456	8	21/07/2007	86.5	20.3	1904
460	8	25/07/2007	87.7	22.6	1932
466	7	31/07/2007	86.6	03.1	1995
485	7	19/08/2007	68.9	05.5	2791
485	8	19/08/2007	11.2	06.0	7815
486	8	20/08/2007	17.9	05.9	7098
488	8	22/08/2007	34.5	05.9	5293
583	12	25/11/2007	84.1	07.5	2636
586	8	28/11/2007	82.0	07.1	2732
595	13	07/12/2007	16.3	06.0	8806
597	13	09/12/2007	34.7	06.1	4587
667	7	17/02/2008	78.3	18.3	2136
669	7	19/02/2008	79.8	18.4	2092
671	8	21/02/2008	81.2	18.6	2063
674	9	24/02/2008	83.0	18.8	2037
675	7	25/02/2008	83.6	18.9	2032
677	5	27/02/2008	84.6	19.2	2026
679	7	29/02/2008	85.6	19.6	2025
681	7	02/03/2008	86.5	20.0	2029
684	9	05/03/2008	87.6	22.0	2042
685	7	06/03/2008	87.8	22.8	2048
686	5	07/03/2008	87.8	23.8	2056
687	11	08/03/2008	87.7	00.8	2064
703	9	24/03/2008	77.5	05.2	2431
709	5	30/03/2008	68.0	05.5	3017
886	11	23/09/2008	76.0	18.2	1997
892	12	29/09/2008	81.0	18.5	1736
894	12	01/10/2008	82.2	18.6	1700

is self-calibrated and the absolute fluxes are not required. Nevertheless, depending on the instrumental properties and the geometry there are some peculiarities to take into consideration; these are described below. Since it is the first time that we publish results from solar occultations by SPICAV UV, the data processing is presented in some detail. SOIR occultations have been already reported several times (Vandaele et al., 2008; Belyaev et al., 2008), thus, the SOIR technique is only briefly described.

2.1. Spectrometer SPICAV-UV

2.1.1. Generalities

The ultraviolet channel of the SPICAV instrument is a spectrometer very similar to the UV channel of the SPICAM (part of the payload of Mars Express orbiter) (Bertaux et al., 2006, 2007a). It operates in the 118–320 nm spectral range with a resolution of 1.5 nm at nadir or stellar/solar occultation modes (Table 2). The intensified CCD matrix of the spectrometer has 384 (spectral columns) × 288 (spatial lines) of useful pixels (in all 408 × 289 pixels). The spectra are registered in columns 9–391 (starting from 0th); columns 393–407 are masked and serve as to retrieve the dark current; 0–7 – for offset level; 8 and 392 – useless pixels.

During one occultation every second a fixed part of the CCD matrix records a signal from the Sun (in N_{ADU} – number of Analog-to-Digital Units), which is grouped spatially in five bands by one chip binning of 2, 4, 8 or 16 lines of the CCD. When pointed to the Sun these bands correspond to different areas of the solar disk and different target altitudes in the Venus' atmosphere. The altitudes of the adjacent bands differ by 0.2–2 km depending on distance to the limb (target point). Thus, every second we obtain five spectra of atmospheric transmission corresponding to different altitudes. During data processing transmissions are derived independently for the each band, and then all spectra are sorted in the order of decreasing altitude. One occultation session (ingress or egress) lasts 2–5 min while the instrument sounds altitudes from −100 to 250 km (with respect to the surface level). This set is divided into three intervals: −100 to 50 km (the dark current), 50–150 km (the atmosphere) and 150–250 (the solar reference spectrum).

2.1.2. Dark current in the UV

Below 50 km LOS of the instrument is considered to be totally eclipsed by dense Venus clouds (slant optical depth >10). In the solar occultation mode the instrument is not sensitive to the limb brightening, which might have an effect below the cloud deck, and to atmospheric emissions (e.g. NO airglow at 200 nm (Royer et al., 2010)). We therefore use the −100 to 50 km data to retrieve the dark current DC_i, which changes with time for each pixel i. The variation of DC_i during the rest of the occultation is extrapolated using the masked pixels – the averaged signal for them is noted M. Monitoring of DC_i and M with time over the −100 to 50 km altitude range enables us to establish the best fit linear approximation:

$$DC_i(t) = A_i \cdot M(t) + B_i. \quad (1)$$

Once the coefficients A_i and B_i are computed for each pixel, dark current can be retrieved and subtracted for all observations of the session, using M readings for each spectrum. To eliminate the noise of $M(t)$, we smoothed M over the time.

In the solar occultation mode detector images the solar disk covering ~10% of the spectrometer's slit. The direct solar radiation is 10^6 stronger than potential scattered light from the limb. Therefore this background signal is negligible comparing to the solar signal and would not contribute to the dark current.

2.1.3. Solar spectrum in the UV

We assume that there is no atmospheric absorption above 150 km, and retrieve the solar reference spectrum from 150 to 250 km data. Taking into account (1), the solar signal in instrument's counts is expressed as

$$F_i(j) = S_i(j) - DC_i(t_j), \quad (2)$$

where $S_i(j)$ – instrument readings, t_j – time of jth observation, i – pixel number. In the considered altitude interval we noted some monotonous change of $F_i(j)$ attributed to a small drift of the LOS over the solar disk. Assuming this drift remains constant during the session we linearly extrapolated F_i to all measurements at altitudes below 150 km. This operation results in the transmission:

$$T_i(t_j) = \left(S_i^A - DC_i(t_j)\right)/F_i(j) \quad (3)$$

where S_i^A – solar light passed through atmosphere (in ADU) at the moment t_j. In parallel, we used the observed solar spectra to establish pixel-to-wavelength assignment comparing with the positions of solar lines measured by SOLSPEC (Thuillier et al., 2009).

2.1.4. Error analysis

Assuming a Poisson statistics of photons detection, we estimated the variance of one pixel measurement as $V = N_{ADU}/K$, where K is a gain factor of CCD's intensifier. Factor K, a number of photons necessary for 1 ADU, is determined from empirical relation $K = 1/\exp(-2.665 + 0.02424HT)$, where HT is the intensifier voltage in telemetry units. The variance for the transmission T is then computed as:

$$V(T) = \sum_k V(x_k)(\partial T/\partial x_k)^2, \quad (4)$$

where x_k denotes the variables of T: N_{ADU}, F, DC. The resulting error bars $\varepsilon(\lambda) = \sqrt{V[T(\lambda)]}$ are shown in Fig. 2b together with measured spectrum; in Fig. 2c relative errors are presented as a ratio $\varepsilon(\lambda)/T(\lambda)$ in (%). The minimal extent of the error bars is about 1–2%, and they are much higher at wavelengths below 220 nm because of low solar flux in that spectral range.

2.2. SOIR spectrometer

SOIR is a high-resolution infrared echelle spectrometer with an acousto-optical tunable filter (AOTF), which is used for the sorting of diffraction orders (Korablev et al., 2004; Nevejans et al., 2006). The instrument is exclusively devoted to solar occultations covering the spectral range of 2300–4500 cm^{-1} (2.2–4.4 μm) with the spectral resolution of ~0.15 cm^{-1} ($\lambda/\Delta\lambda \sim 20{,}000$) (Table 2). Detailed description, in-flight performance and calibrations of the spectrometer are given in papers by Nevejans et al. (2006) and Mahieux et al. (2008). Here we describe briefly the main parameters of the instrument and some features related to SO_2 detection.

The spectrometer's FOV (30 by 2 arcmin) is projected into the detector's 256 × 320 matrix. Registered radiance is dispersed by the echelle grating onto 320 spectral columns, and the diameter of the Sun corresponds to only 24 pixel rows. Typically the 24 rows

Table 2
SO_2 detection by SPICAV UV and SOIR occultations.

	SPICAV UV	SOIR
Spectral range	118–320 nm	2300–4500 cm^{-1} (2.2–4.4 μm)
Spectral resolution	1.5 nm ($\lambda/\Delta\lambda \sim 150$)	0.15 cm^{-1} ($\lambda/\Delta\lambda \sim 20{,}000$)
Vertical FOV	2.5 arcmin	2 arcmin
SO_2 absorption bands	190–230 nm	2480–2520 cm^{-1} (3.97–4.03 μm)
Altitudes of SO_2 detection	85–110 km	65–80 km

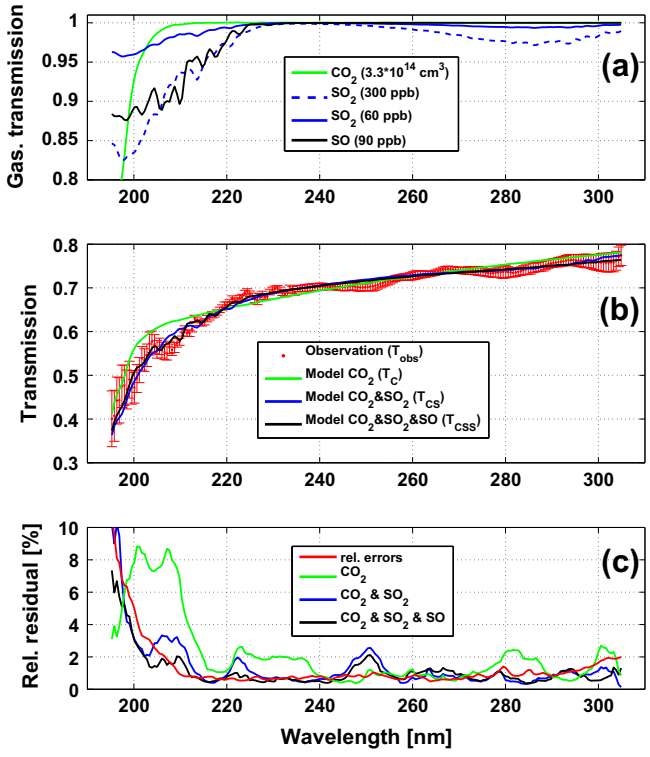

Fig. 2. Example of one SO and SO_2 retrieval from a UV measurement at 93 km (Orbit 361). Models of gaseous transmission (a) include: CO_2 (green), SO_2 (blue), SO (black). The observed transmission T_{obs} (red) is compared with three variants of best fitting (b): without SO_2 and SO (green curve T_C); without SO (blue curve T_{CS}); all together CO_2, SO_2 and SO (black curve T_{CSS}). Relative residuals (c) between the observation and models are presented on a background relative error bars (red). Models are calculated for concentrations: $N_{CO2} = 3.3 \times 10^{14}$ #/cm^3, mmr(SO_2) = 300 ppbv and 60 ppbv, mmr(SO) = 90 ppbv. (For interpretation of the references to color in this figure legend, the reader is referred to the web version of this article.)

are binned into 2 spectra, 12 rows in each. Every second one data package is obtained, containing four couples of spectra with different spectral intervals. The four intervals can be selected among different echelle orders (between 104 and 204), by electrical tuning of the AOTF's radio-frequency. This filter's passband of ~25 cm^{-1} is slightly larger than the spectral width of a single order. Moreover, the spectral profile of the AOTF contains side lobes, extending over a few adjacent orders that results in their mixing and, therefore, distorts the measured spectrum. For the SO_2 study, observations in the spectral range 2480–2520 cm^{-2} (3.97–4.03 μm) are only suitable (orders 111 or 112) (Belyaev et al., 2008). Other measured spectral intervals are not used in our analysis.

In order to obtain the atmospheric transmission in the IR, the reference solar spectrum was derived in the same way as for the UV (see Section 2.1.3). To determine the pixel-to-wavelength assignment we could use the solar lines positions (Belyaev et al., 2008). However, a more precise assignment is obtained from the regular absorption structure of CO_2 around 4 μm (2500 cm^{-1}) (Fig. 4). Other features related to SOIR data reduction, such as the detector dark current non-uniformity, the AOTF spectral profile, and the AOTF frequency-to-wavelength assignment, we refer to papers of Mahieux et al. (2008, 2010).

3. Modeling and retrievals

3.1. General concept

To retrieve the gaseous contents from a transmission spectrum of the atmosphere we apply an inverse method, including forward model, spectral inversion, and vertical inversion. The goal of the forward model is to provide synthetic atmospheric transmissions for each measurement in the spectral ranges of interest. Atmospheric transmission follows the Beer–Lambert's law:

$$T_{mod}(\lambda, z) = \exp[-\tau(\lambda, T, p)], \quad (5)$$

where $\tau(\lambda,T,p)$ is the atmospheric extinction, which generally depends on wavelength λ, temperature T and pressure p at specified altitude z. The extinction is computed taking into account contributions from several gaseous and aerosol species:

$$\tau(\lambda, T, p) = \sum_i N_i \sigma_i(\lambda, T, p) + \tau_{aer}(\lambda, T, p), \quad (6)$$

N_i – slant column density of ith gas (number of molecules/cm^2), $\sigma_i(\lambda,T,p)$ – molecular extinction cross-sections (absorption or scattering) (cm^2), $\tau_{aer}(\lambda,T,p)$ – aerosol extinction.

At the first step we perform the spectral inversion: retrieval of the slant column densities N_i from the model $T_{mod}(\lambda,z)$ by comparison with observed transmission $T_{obs}(\lambda,z)$ at each altitude. The fitting procedure is based on Levenberg–Marquardt algorithm with several parameters (N_i, τ_{aer}) (Markwardt, 2009), where best estimates of (N_i,τ_{aer}) and their error bars are found by minimizing the χ^2-function:

$$\chi^2 = \sum_j [(T_{obs}(\lambda_j) - T_{mod}(\lambda_j))/\varepsilon(\lambda_j)]^2 \quad (7)$$

$\varepsilon(\lambda_j)$ are estimated errors of the measured transmission for all spectral points λ_j. However, the spectrum T_{obs}, determined by formula (3), is the ratio of two measured spectra that are convolved by the spectral instrument function (PSF). On the other hand, T_{mod} is initially calculated at a quite high spectral resolution not taking into account the PSF. In order to simulate actual (convolved) transmission $\breve{T}_{mod}(\lambda)$ we apply following formula:

$$\breve{T}_{mod}(\lambda) = \frac{\int PSF(\lambda' \to \lambda) T_{mod}(\lambda') \widehat{F}(\lambda') d\lambda'}{F(\lambda)}, \quad (8)$$

where $\widehat{F}$ is the result of de-convolution of the measured solar spectrum F (formula (2)); integration with the PSF is computed for high resolution coordinate λ'. De-convolution of F is based on Richardson–Lucy method (Lucy, 1974).

In the second step we apply the vertical inversion, retrieving gaseous local densities from horizontal slant densities. Assuming the spherical symmetry and the hydrostatic equilibrium in the atmosphere we used the "onion peeling" method (Vandaele et al., 2008). To account the vertical continuity of the measured density profiles, reducing the retrieval errors, we performed a Tikhonov's regularization technique as was described for our application by Quemerais et al. (2006).

3.2. UV transmission

Since at $\lambda < 180$ nm the signal from solar radiance is too weak, we considered only the atmospheric transmission at longer wavelengths. In Fig. 1 the extinction cross-sections are presented for gases that were taken into account in the forward model. There are a few absorption bands of sulfur oxides' molecules in SPICAV UV spectral range: electronic transition bands $B^3\Sigma^- - X^3\Sigma^-$ (190–240 nm) and $A^3\Pi^- - X^3\Sigma^-$ (240–260 nm) of the monoxide (Colin, 1969), and electronic transition bands $\widetilde{C}^1B_1 - \widetilde{X}^1A_1$ (190–235 nm) and $\widetilde{B}^1B_1 - \widetilde{X}^1A_1$ (250–340 nm) of the dioxide (Wu et al., 2000; Rufus et al., 2003). We emphasize the available pack of spectral data for SO (the first band) (Phillips, 1981); at wavelengths longer than 235 nm we did not find any reference to extract cross-sections. Thus, it was decided to extrapolate Phillips' results beyond 235 nm by parabolic law in logarithmic scale as most

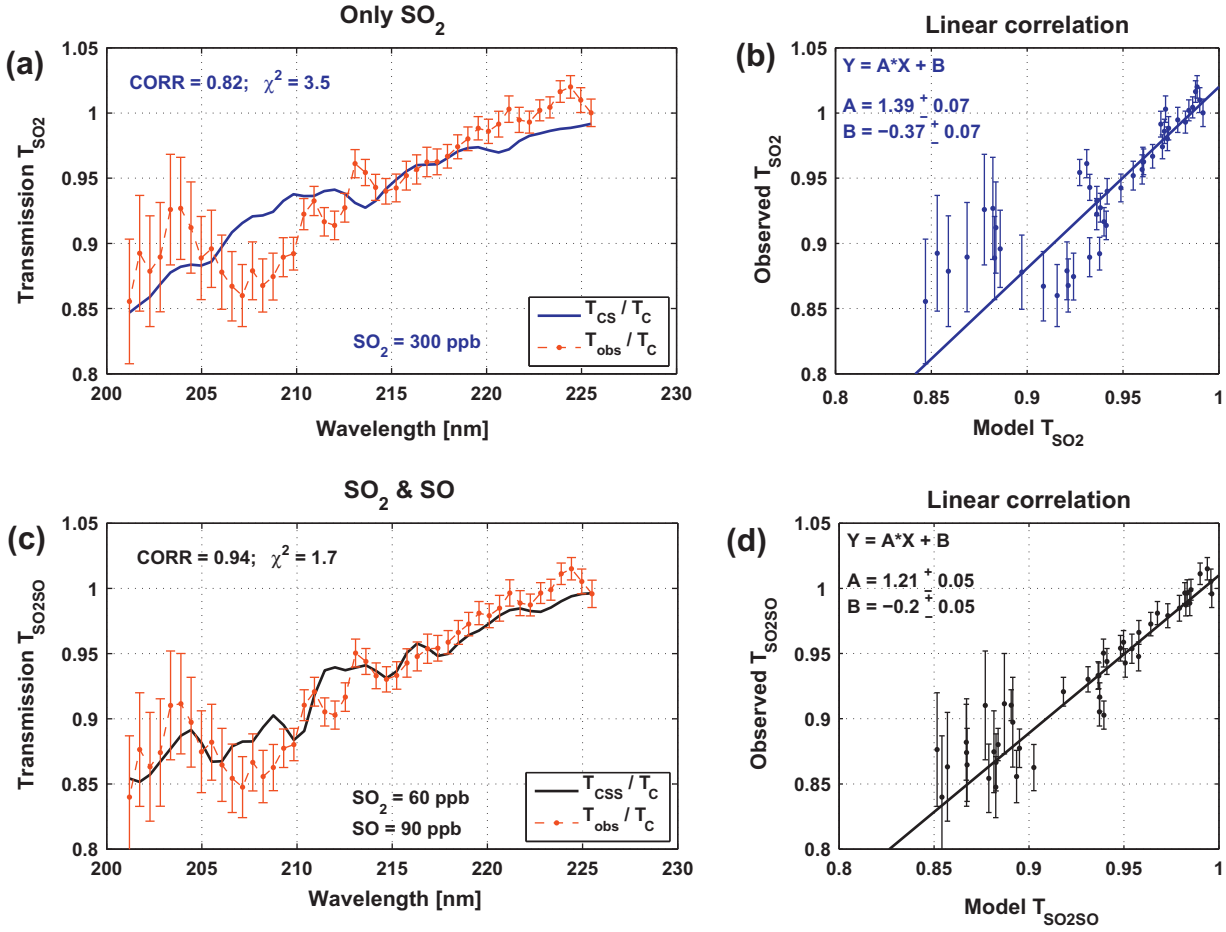

Fig. 3. Correlation analysis at 201–226 nm to distinguish SO_2 and SO absorption features. Models of transmission spectra for only SO_2 (a) and for SO_2 and SO (c) are compared with observed ratio T_{obs}/T_C (correlation coefficient CORR and normalized χ^2 value are shown for both cases). "Scatter plots" (b and d) present linear correlation between data and model with coefficients A and B from least squares method. (For interpretation of the references to color in this figure legend, the reader is referred to the web version of this article.)

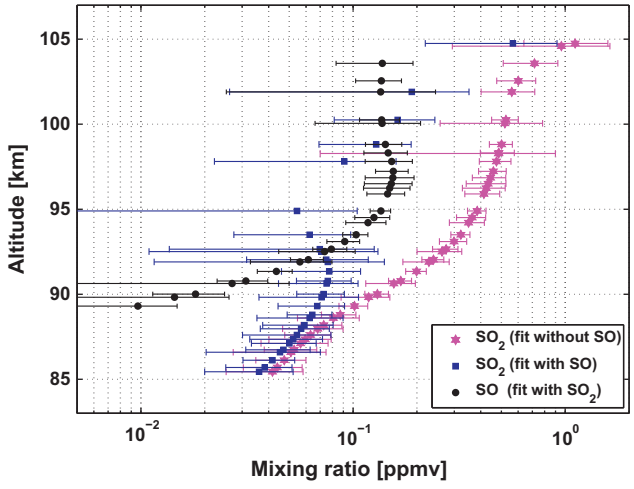

Fig. 4. An example of SO_2 and SO retrievals from one occultation sequence by SPICAV UV (Orbit 361). Black and blue profiles indicate SO and SO_2 mixing ratios obtained together in the fitting procedure. Magenta profile presents SO_2 content derived without contribution of SO. Error bars are given at 2-sigma. (For interpretation of the references to color in this figure legend, the reader is referred to the web version of this article.)

harmless way to represent the shape of the continuum of the band versus SO_2, which has another band system. Spectral resolution of SO cross-sections is 0.08 nm, while for SO_2 it is 0.05 nm; they are 2–3 times less than the width of the instrument function, and it allows us to distinguish local spectral features between these gases.

The absorption cross-sections of carbon dioxide were taken from Parkinson (2003), while for the CO_2 Rayleigh scattering we used recent measurements of Ityaksov et al. (2008). All the data shown in the Fig. 1 correspond to the temperature of 195 K, while the expected temperature at Venus is 180–200 K. For the carbon dioxide the cross-sections at 295 K are also available, and we used interpolation and extrapolation in the range of 180–200 K when performing the spectral inversion. Lacking temperature dependence, the SO_x cross-sections were assumed to be constant. To account for the spectral behavior of aerosols, we considered the extinction of the slant optical thickness (opacity) as $\tau_{aer}(\lambda) = \tau_{\lambda o}(\lambda_o/\lambda)^{\alpha}$. Here α is the Angström coefficient and λ_o is a reference wavelength (Montmessin et al., 2006).

The spectral inversion consisted of simultaneous fitting of the following four parameters: N_{SO2}, N_{SO}, λ_o and α. To facilitate the retrieval, the CO_2 column density N_{CO2} was considered known and taken from SOIR data for the same occultation. SOIR CO_2 densities had been readily retrieved from the 4-μm band in a large altitude range 65–120 km.

Analyzing the spectral dependence of the sulfur oxides cross-sections (Fig. 1) one may notice that the SO band is fully overlapped by the SO_2 band at 200–230 nm, but SO_2 has an additional structure at 270–310 nm, which could be used for a separate retrieval with no influence from SO absorption. However, this band alone (without

the main band at 200–230 nm) was found to be too weak for dependable spectral inversion. It is demonstrated in Fig. 2a, showing synthetic spectra computed for gaseous concentrations derived from the considered measurement. The spectra are convolved with the instrument contour with a width of 1.5 nm (Table 2). In order to distinguish the SO_2 absorption from CO_2, and SO from SO_2, three iterations of the spectral inversion were performed at each altitude. On the first step the spectrum was fitted with only CO_2 and aerosol: $T_{mod}(\lambda) = T_C(\lambda)$. In the second iteration we added some SO_2 absorption into the $T_C(\lambda)$, fitting parameters $\tau_{\lambda o}$, α and N_{SO2}: $T_{mod}(\lambda) = T_{CS}(\lambda)$. And finally, on the last step, transmission adjustment together with N_{SO} was performed: $T_{mod}(\lambda) = T_{CSS}(\lambda)$. In Fig. 2b comparison of all three iterations with the observed transmission $T_{obs}(\lambda)$ is presented for one example measurement at 93 km. Analyzing residuals of the transmission $|1 - T_{obs}(\lambda)/T_{mod}(\lambda)| \cdot 100\%$, we found that the third fit $T_{CSS}(\lambda)$ was the best, therefore confirming the SO detection (Fig. 2c). The largest difference between SO_2 and SO absorption features is apparent in the intervals 201–212 nm and 219–226 nm, while at 212–219 nm the features are almost similar. To confirm the reality of the absorption due to SO we performed correlation analysis in these particular spectral ranges, demonstrating that SO significantly improves the shape of transmission spectrum (Fig. 3).

Such accurate study was done for ratios $T_{SO2}(\lambda) = T_{CS}(\lambda)/T_C(\lambda)$ and $T_{SO2SO}(\lambda) = T_{CSS}(\lambda)/T_C(\lambda)$ that express models of transmissions with only SO_2 and including both SO_2 and SO (Fig. 3). We compared those spectra with observed ratio $T_{obs}(\lambda)/T_C(\lambda)$, which indicates a part of transmission responsible for SO_2 or SO_2 and SO absorption (Fig. 3a and c). Calculations of Pearson's correlation coefficient CORR and χ^2 value make us sure that SO really improves the shape of transmission spectrum in intervals 201–212 nm and 219–226 nm. Value χ^2, which is twice as less in the SO case, was estimated using formula (7) and normalized by $(N - p)$, where N is number of spectral points, p is number of fitted parameters ($N = 50$, $p = 4$ for $T_{SO2}(\lambda)$ and $p = 5$ for $T_{SO2SO}(\lambda)$). From the other hand, we created a "scatter plot" for both cases – dependence of measured points on theoretical (Fig. 3b and d). Linear law coefficients A and B were found by weighted least square method; in perfect case $A = 1$, $B = 0$. In our example these coefficients are respectively closer to verity for SO variant than for SO_2.

Applying the three-iteration algorithm for all measured altitudes, and performing then the vertical inversion, we retrieve the altitude profiles of SO_x mixing ratios. In Fig. 4 the result from one occultation is shown (Orbit 361, 17 April 2007). The SO_2 profiles are retrieved for two cases: fitting without and with SO. The main differences between the two SO_2 profiles are: (1) the SO_2 abundance decreases when SO is included; (2) SO appears only above ~90 km, and it is anti-correlated with SO_2 at higher altitudes – decreasing trend of SO_2 is accompanied by increasing trend of SO and reversely. All error bars are given at 2-sigma.

3.3. IR transmission

In the IR range, where the molecular absorption lines are sensitive to the temperature, we use line-by-line calculations for gaseous cross-sections with line parameters taken from the HITRAN 2004 spectroscopic database (Rothman et al., 2005). A procedure to retrieve the SO_2 mixing ratio from SOIR 4 μm data is described by Belyaev et al. (2008). Here we report modifications introduced in order to improve the accuracy of retrievals.

Around 4 μm a conspicuous regular structure of carbon dioxide masks the SO_2 signature (Fig. 5). On the other hand, CO_2 structure could be used for instrumental corrections decreasing systematic errors. During an occultation the temperature inside the instrument may change by 2–4 °C. It results in wavelength shifts of both the spectrometer, and the AOTF. As the first step, to establish a pixel-to-wavenumber assignment, we compare spectra recorded at

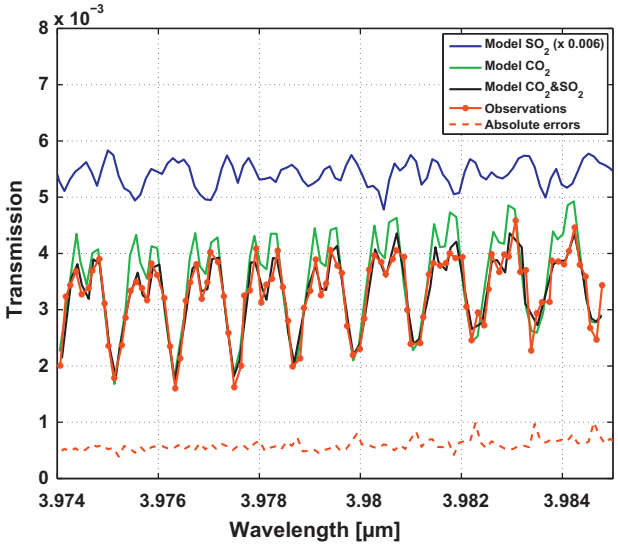

Fig. 5. Comparison of an observed transmission at 68 km (Orbit 361) (red solid) with two variants of best fitting in the IR: without SO_2 (green curve) and with SO_2 (black curve). Blue curve is model of only SO_2 gaseous transmission (multiplied by 0.006) for mixing ratio 350 ppb. Red dashed line is spectral distribution of absolute errors for the given measurement. (For interpretation of the references to color in this figure legend, the reader is referred to the web version of this article.)

altitudes above 85 km with a synthetic model, assuming the CO_2 density from VIRA-2 database (Zasova et al., 2006) and absence of SO_2. To simulate the distortion of a spectrum due to the AOTF side lobes (see above), a superposition of ±5 echelle orders was included in the model according to the AOTF profile and the dispersion curve (Mahieux et al., 2008). We fitted the dependence of wave number on pixel number by a square function and extrapolated its coefficients to altitudes below 85 km. In the second step we adjusted the spectral position of the AOTF profile's peak wn_o. It affects the apparent depth of the carbon dioxide lines, and, therefore, wn_o was fitted together with N_{CO2} at altitudes above 85 km (assuming again $N_{SO2} = 0$). Then wn_o was extrapolated to the altitudes below 85 km by a linear law. Implementing the above corrections decrease systematic errors by ~10% with respect to the results reported in Belyaev et al. (2008).

At the last step the spectral inversion was performed with simultaneous fitting of N_{CO2} and N_{SO2} in the whole altitude range 65–120 km. In Fig. 5 an example of one SO_2 retrieval is presented: the observed transmission spectrum at 3.974–3.986 μm (order 112) is compared with the synthetic model for two cases, including and not including SO_2. The model of SO_2 transmission is presented as well to see SO_2 lines position in the measured spectrum. Spectral distribution of absolute errors for the measurement is shown in the same figure separately from the spectrum. The analysis of residuals (in a way similar to SPICAV UV) makes us confident about a positive detection of sulfur dioxide as at the altitude 68 km as well as in the whole detection range 65–80 km. In order to distinguish SO_2 signatures on the background of much stronger CO_2 structure, an additional correlation study with "scatter plots" was done as described by Belyaev et al. (2008). As a result altitude profiles of local densities were retrieved in range 65–80 km for SO_2 and 65–120 km for CO_2. Slant column densities of carbon dioxide N_{CO2} obtained from SOIR were used for the SPICAV UV spectral inversion at the same occultation between 85 and 110 km (see Section 3.2).

4. Results and discussion

The retrieval procedure in the UV range described above results in the three mixing ratio profiles of SO_x components for each

occultation: SO_2 without contribution of SO; SO_2 in presence of SO; SO in presence of SO_2 (see Fig. 4 and Section 3.2). The retrieved abundance of SO_2 is considerably reduced above 90 km if SO is allowed to explain the observed absorption spectrum. In the lower altitude range probed in the UV (85–90 km), where SO content is significantly less, the retrieved abundance of SO_2 is independent on SO. An anti-correlation of the SO and SO_2 profiles could be interpreted as an evidence of an active sulfur photochemistry in the Venus atmosphere, well above the clouds. If we do not allow SO in the spectral retrieval, SO_2 abundance becomes too high above 85 km, requiring extreme assumptions to explain, e.g. supersaturation of H_2SO_4 vapor (Zhang et al., 2010) associated with its large photolysis rate. The considered example is taken from one particular session at Orbit 361 (see Table 1). The full set of all occultations together demonstrates high variability of SO_x content along the whole altitude range. To establish a general statistics and clarify the origin of the variability, we sorted our vertical profiles in various groups defined by geographical, temporal or temperature criteria (see Sections 4.1–4.3). It is also reasonable because for some occultation sequences just a few values were retrieved, poorly constraining the profile. Associated with others measurements such data would contribute to characterization of general trend of SO_x profiles.

Most of the profiles (Figs. 6–8) exhibit two layers of SO_2 abundance: the lower layer (65–80 km) determined by SOIR measurements, and the upper one (85–105 km) observed by SPICAV UV. Below 65 km any signal from the Sun is undetectable because of cloud extinction. Above 80 km the sulfur dioxide is undetectable in the IR at 4 μm, where its cross-section is much weaker than in UV. In the UV range both the SO_x cross-sections and aerosol opacity are much stronger, so the solar radiation is obscured by the aerosol extinction below 85 km but the absorption due to SO_x is measurable above.

4.1. Dependence on latitude and local time of Venus

Since the SO_2 molecule is destroyed by photolysis, its content is expected to vary with Venus local time, a particularly large difference is observed between night and day sides, for example, the SO_2/SO ratio at the night side 100 times more than at the dayside above 85 km (Sandor et al., 2010). In solar occultation the instrument always sounds the twilight atmosphere, where physical conditions are different from the day or night. From our occultations we sorted data by local time: LT < 12:00 (Fig. 6a and c), LT > 12:00 (Fig. 6b and d); and by latitude: Lat > 50° (Fig. 6a and b), Lat < 50° (Fig. 6c and d). In the polar region there is no large difference among day and night, the isolation is almost invariable, and the distribution by local time is not meaningful. In the low latitudes the SO_2 mixing ratio at 65–70 km is higher than in the polar region; at the same time there are no significant variations between morning and evening. The latitudinal behavior is generally characterized by decrease SO_2 content from the equator to the Pole that is in qualitative correlation with SPICAV UV nadir results reported by Marcq et al. (2011a). This trend is connected with the same latitudinal decrease of the Venus' cloud top level and, therefore, an additional study about SO_2 production from aerosol particles is required: either it comes from sulfur's evaporation or from H_2SO_4 (Sandor et al., 2012; Zhang et al., 2012).

Scale height of the SO_2 density was calculated for altitudes 70–80 km: 3.5 ± 0.5 km at latitudes >50°N, and 4.1 ± 0.7 km at latitudes <50°N. In the upper sulfuric layer (except evening in equator, where we have very poor dataset) an X-shape SO–SO_2 profiles structure is observed indicating photochemical activity of both gases.

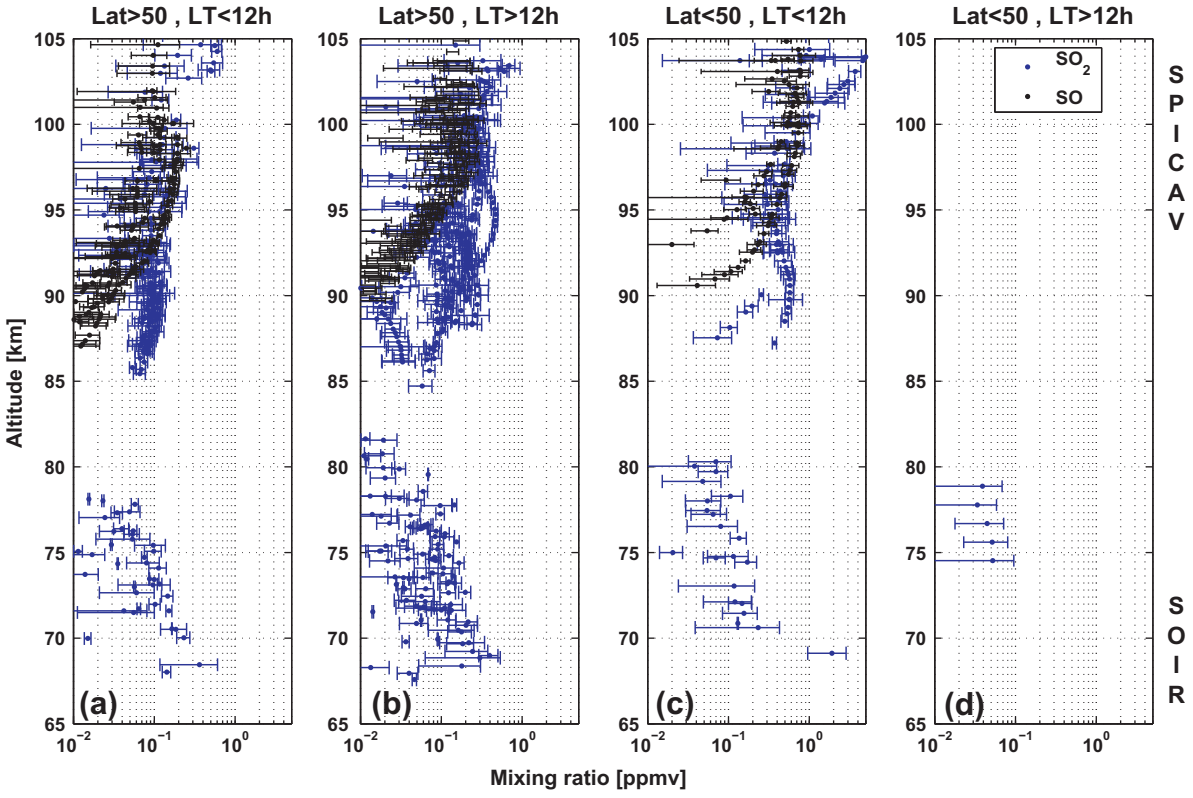

Fig. 6. Sorting of SO (in black) and SO_2 (in blue) mixing ratios by latitude and local time: (a) morning in Northern Pole (Lat > 50°, LT < 12 h); (b) evening in Northern Pole (Lat > 50°, LT > 12 h); (c) morning in equatorial region (Lat > 50°, LT < 12 h); (d) evening in equatorial region (Lat > 50°, LT < 12 h). Values below 80 km are from SOIR measurement, while values above 85 km are from SPICAV UV. (For interpretation of the references to color in this figure legend, the reader is referred to the web version of this article.)

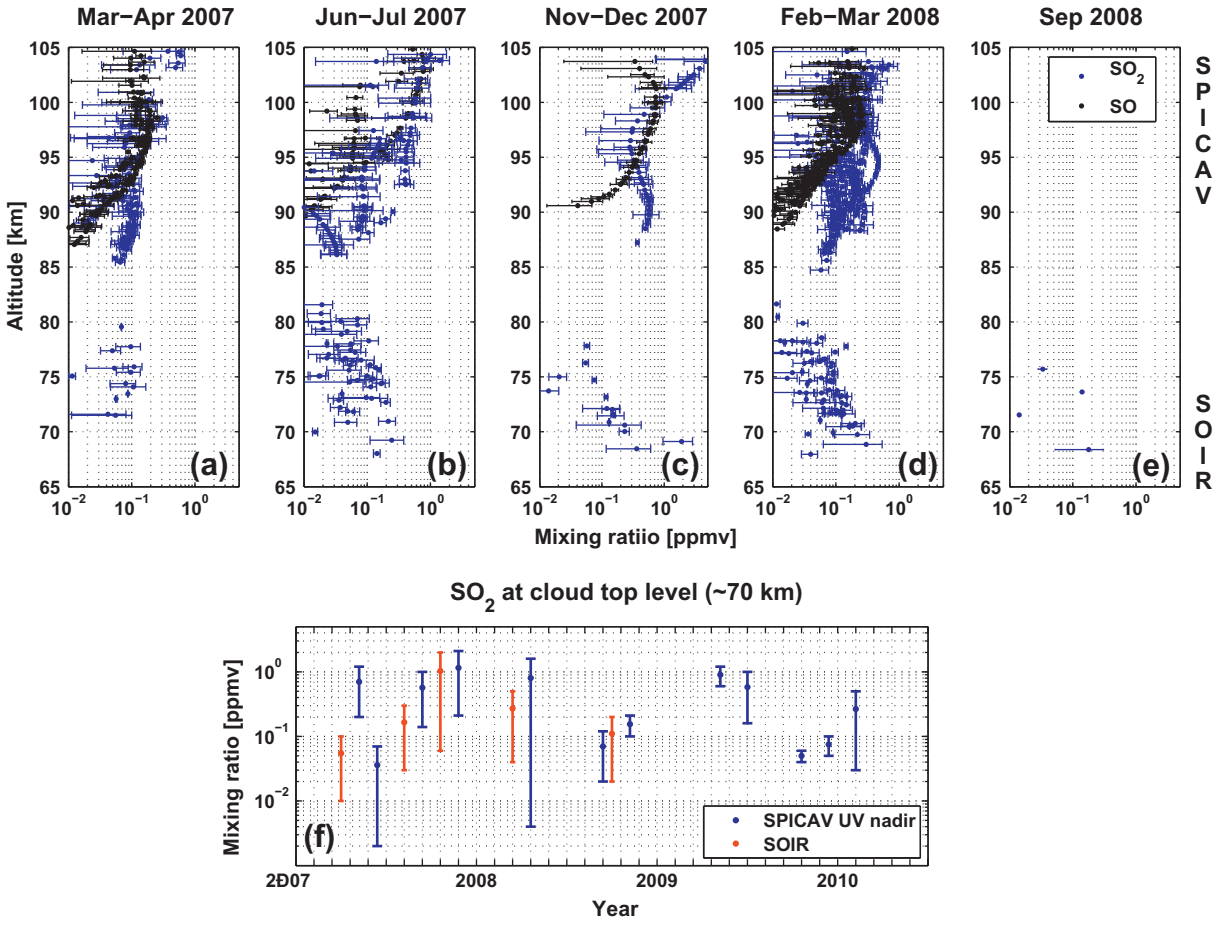

Fig. 7. Sorting of SO (in black) and SO_2 (in blue) mixing ratios by annual time: (a) March–April 2007; (b) June–August 2007; (c) November–December 2007; (d) February–March 2008; (e) September 2008. Values below 80 km are from SOIR measurement, while values above 85 km are from SPICAV UV. Block (f) shows annual evolution of SO_2 content at cloud top level (~70 km) retrieved from SOIR occultations (red) and from SPICAV UV nadir observations (blue) (Marcq et al., 2011b). (For interpretation of the references to color in this figure legend, the reader is referred to the web version of this article.)

4.2. Interannual variability

As described in Section 1 and mentioned in previous papers (e.g. Mills et al., 2007), a steady decline of SO_2 abundance at Venus' cloud top was observed from 500 ppbv in 1978 to 20 ppbv in 1995. Then, the first results from SOIR occultations in 2006–2007 gave again ~500 ppbv around 70 km, the increase resembling the one in 1978 (Belyaev et al., 2008). Three possible explanations of such behavior were suggested: active volcanism (Esposito, 1984); changes in the effective eddy diffusion within the cloud layer (Krasnopolsky, 1986, p. 147); changes in atmospheric dynamics (Clancy and Muhleman, 1991). With the new SPICAV/SOIR occultation measurements we can continue tracking this evolution at cloud top level in the time interval from March 2007 to September 2008.

In Fig. 7 we sorted SO_2 and SO profiles in five groups by months: March–April 2007 (a); June–August 2007 (b); November–December 2007 (c); February–March 2008 (d); September 2008 (e). At the ~70 km level the temporal variability of SO_2 mixing ratio qualitatively and quantitatively confirms the results of SPICAV UV nadir observations (Marcq et al., 2011b): from 0.05 ppm in the first half of 2007 to 0.1–0.2 ppm in the second half of 2008 (Fig. 7f). Data in the Fig. 7f indicate limits of detections collected from all available point for each time interval. In the upper layer around 95 km the mixing ratio also increases from ~0.1 ppm to ~0.5 ppm keeping the X-shape structure almost stable.

4.3. Dependence on temperature in upper layer

Basically, we detect two layers of SO_2, one at 65–80 km, and one at 85–105 km. The lower layer is the upper tail of the SO_2 portion embedded in the clouds, which is also observed with UV nadir viewing. It declines with increasing altitude, as the result of the photodissociation, when unprotected by the clouds from the solar UV radiation. The upper layer detected (above the clouds, but within the upper haze) is characterized by a significant SO_2 increase with altitude from 85 to 105 km, which calls for a new source of SO_2 implying a downward flux of SO_2 around 100 km. One possible source of SO_2 production in the upper haze layer could be photodissociation of H_2SO_4 vapor resulting from evaporation of the acid aerosol droplets. The product SO_3 can be further destroyed by light to yield sulfur dioxide. This scheme was recently proposed by Zhang et al. (2010, 2012), who explored different regimes of the H_2SO_4 photolysis. The idea deals with the dependence of the production rate of SO_2 on the actual density of H_2SO_4, whose saturation pressure is a highly varying function of temperature. The warmer is the environment, the higher may be the number density of H_2SO_4 in the gaseous phase (because of evaporation from droplets) finally providing a more abundant SO_2 and SO layer. In the present work we have facility to check this hypothesis on a basis of temperature behavior of sulfur oxide's contents.

Using SOIR occultations there is a possibility to retrieve the atmospheric temperature from CO_2 rotational temperature for various altitudes (Mahieux et al., 2010). Here we considered the

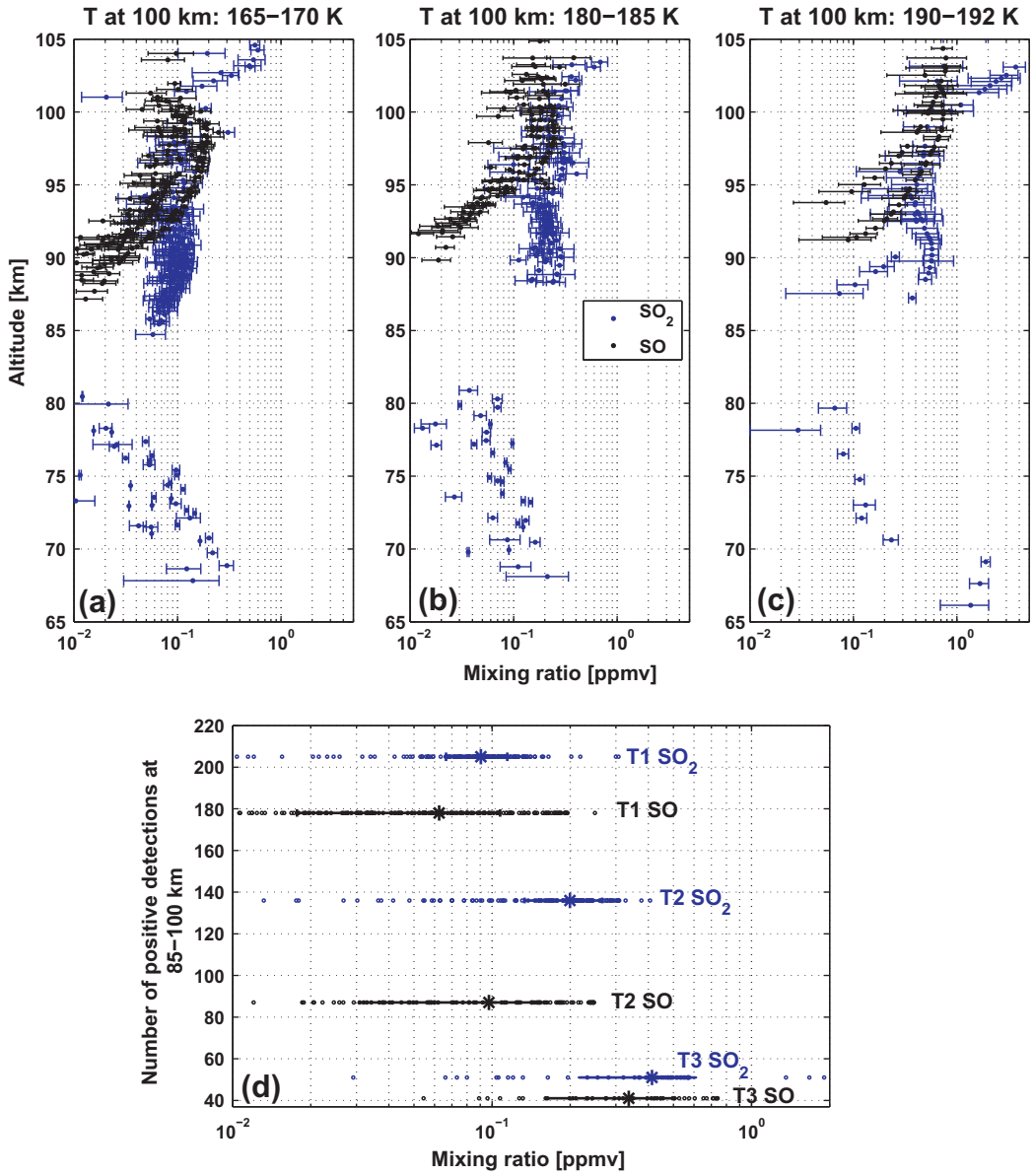

Fig. 8. Sorting of SO (in black) and SO_2 (in blue) mixing ratios by temperature at 100 km: (a) 165–170 K; (b) 180–185 K; (c) 190–192 K. Values below 80 km are from SOIR measurement, while values above 85 km are from SPICAV UV. Block (d) shows statistics of positive SO and SO_2 detections at all three regimes: T1 165–170 K; T2 180–185 K; T3 190–192 K. Points are taken in 85–100 km range with median values and median absolute deviations. (For interpretation of the references to color in this figure legend, the reader is referred to the web version of this article.)

region around 100 km. For most of selected orbits we obtained averaged temperatures in the range 95–105 km and sorted the data in three groups: 165–170 K; 180–185 K; 190–192 K. Retrieved SO_2 and SO profiles at these temperature bins are presented in Fig. 8a, b and c respectively. The most frequent is the coldest thermal case (a), and it is quite stable: a large number of points concentrate in the upper layer with little deviations. There are fewer observations for the second case (b) and just a few measurements for the warmest case (c). The full statistics of SO and SO_2 positive detections is shown in Fig. 8d with median values and deviations. We conclude that in the altitude range 90–100 km the SO_2 mixing ratio increases with temperature: from 0.1 ppmv at 165–170 K to 0.5–1 ppmv at 190–192 K. SO content also increases, keeping the X-shape SO–SO_2 profiles structure constant.

In order to analyze those three thermal regimes, the corresponding SO and SO_2 profiles, were compared with two models developed by Zhang et al. (2010, 2012). Model 1 was calculated for the H_2SO_4 saturation ratio of 0.25 (Zhang et al., 2012), while model 2 is for a ratio equal to 10 with the same temperature profile (Zhang et al., 2010). The second case is a supersaturation event, when sulfuric acid abundance is larger than its saturation vapor pressure by an order of magnitude. That would increase the photolysis production of SO_3 and, therefore, provide the upper layer with molecules of SO_x. In Fig. 9 the coldest observed temperature case T1 is closer to the model 1 – such conditions seems to be more stable and probable. The warmest case T3 is closer to the model 2, but the difference of temperature between T1 and T3 (about 25°) implies a large increase of H_2SO_4 saturation pressure, which means that supersaturation is not necessary for warm conditions (and large SO_2 content); see Zhang et al. (2010), their Fig. S1 in Supplementary material. These episodes of high temperature at terminator may be caused by adiabatic descent of air, which is frequently detected on the night side from stellar occultations (Bertaux et al., 2007b). We also compared SPICAV/SOIR results with ground-based JCMT measurements by Sandor et al. (2010) that are found to correlate with our case T1 in the upper layer. The mean result of the

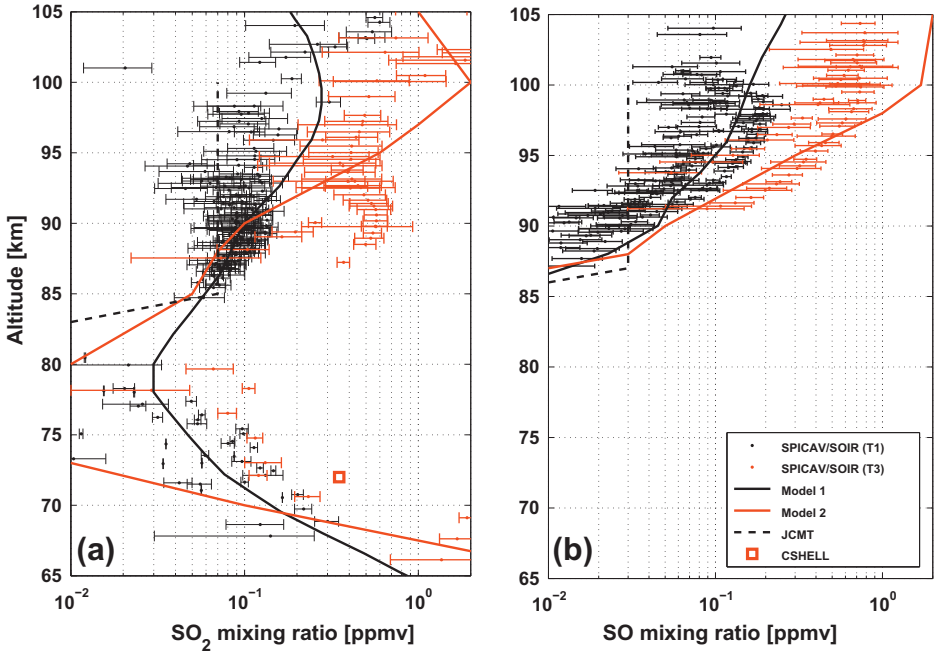

Fig. 9. Comparison of measured SO_2 (a) and SO (b) mixing ratio profiles with two types of model (1 and 2). SPICAV/SOIR data are taken from Fig. 8 at two temperature regimes for 100 km level: T1 (black points) 165–170 K; T3 (red points) 190–192 K. Results from ground-based observations are marked by black dashed lines (JCMT data; Sandor et al., 2010) and by a red square from the CSHELL (Krasnopolsky, 2010). Models 1 (black solid) and 2 (red solid) were calculated at different regimes of H_2SO_4 photolysis around 100 km (mod. 1: Zhang et al., 2012; mod. 2: Zhang et al., 2010). (For interpretation of the references to color in this figure legend, the reader is referred to the web version of this article.)

SO_2 retrieval from the 4 μm band by ground-based high-resolution spectrograph CSHELL (Krasnopolsky, 2010) is in agreement with SOIR observations around 72 km (Fig. 9a).

4.4. The ratio $[SO_2]/[SO]$

One critical aspect of the sulfur photochemistry is the interconnection between SO_2 and SO molecules. In the paper by Zhang et al. (2010) it is shown that at altitudes 90–100 km the dominant mechanism for SO_2 production is the oxidation of SO, and it is destroyed by the photolysis returning back to the monoxide. Both reactions have similar rates at the altitudes of interest: $\sim 5 \times 10^4\ cm^{-3}s^{-1}$ (for the model 1) and $\sim 5 \times 10^5\ cm^{-3}s^{-1}$ (for the model 2). From the balance of SO, the monoxide production (excluding the SO_2 photolysis) is fed by oxidation of sulfur, and destruction is through dissociation to S + O. Rates of these two reactions have the same order of magnitude as for the dioxide's production and dissociation. All other reaction rates involved are much smaller. It means that the concentration ratio $[SO_2]/[SO]$ at 90–100 km in presence of the solar light should be close to unity, and would not depend neither on temperature nor on H_2SO_4 concentration (however, it depends on the solar flux).

We calculated the $[SO_2]/[SO]$ ratio for all profiles of Fig. 9. This ratio for four cases (T1, T3, model 1 and model 2) was found to vary from 0.5 to 5 at altitudes 90–100 km (Fig. 10), which is compatible with day side JCMT results (Sandor et al., 2010) and with models proposed by Yung and DeMore (1982).

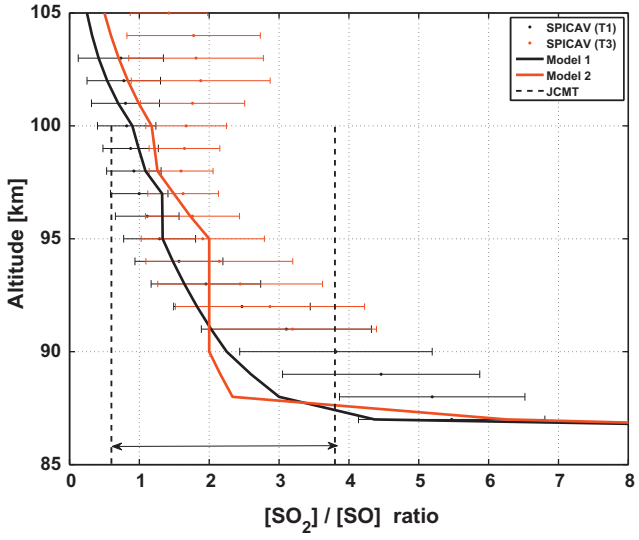

Fig. 10. Vertical distribution of $[SO_2]/[SO]$ ratio measured by SPICAV UV at two temperature regimes around 100 km: T1 (black points) 165–170 K; T3 (red points) 190–192 K. JCMT data (black dashed) are marked as bar of the ratio variability in the day side (Sandor et al., 2010). Models 1 (black solid) and 2 (red solid) were calculated at different regimes of H_2SO_4 photolysis around 100 km (mod. 1: Zhang et al., 2012; mod. 2: Zhang et al., 2010). (For interpretation of the references to color in this figure legend, the reader is referred to the web version of this article.)

4.5. H_2SO_4 or S_x as a source of SO_2 in the upper haze layer

Discussions above about possible source of sulfur dioxide around the upper haze are linked to photolysis of H_2SO_4 vapor produced from evaporation of the acid aerosol droplets. This hypothesis looks in agreement with our SO_2 distribution at 85–100 km (see Section 4.3 and paper of Zhang et al. (2012)). However, recent upper limit detections of H_2SO_4 from sub-mm groundbased measurements make Zhang's theory less likely (Sandor et al., 2012). The limit around 3 ppbv was established that is quite not enough to generate 0.1 ppmv of SO_2 abundance at the upper layer. In parallel, the same opinion is proposed by Krasnopolsky (2011) on a basis of H_2SO_4 vapor calculations at 70–110 km. Sandor in his mentioned paper suggests sulfur S_x as one of influential reservoirs for SO_2 production. This idea is also developed by Zhang et al. (2010, 2012): sulfur dioxide arises from evaporation of S_x aerosol particles and further oxidation forming SO. Nevertheless, pro and contra analysis

made by Zhang et al. (2012) shows the sulfur version as less probable. To resolve our problem an additional study about existence of S_x and/or H_2SO_4 aerosol haze around 100 km is required; real measurements of SO_3 abundance are also needed in sense of the $H_2SO_4 \rightarrow SO_2$ transition.

5. Conclusions

We analyzed SPICAV/SOIR solar occultation spectra and extracted spectral transmissions in the 170–320 nm interval with a resolving power $R \sim 200$ and in 3970–4030 nm at $R \sim 20{,}000$. We compared the measured spectra with forward models for transmissions in UV and IR ranges, and retrieved the altitude profiles of SO_2 and SO content above Venus' clouds: at 65–80 km with SOIR spectrometer, and at 85–105 km with SPICAV UV. Our main results are:

(1) There are two SO_2 layers in Venus' mesosphere: $0.2 \rightarrow 0.02$ ppmv at 65–80 km and $0.05 \rightarrow 2$ ppmv at 85–105 km, with most likely very little SO_2 content in the range 80–85 km, considering the observed vertical gradients at 80 and 85 km, which have different signs. In the upper layer we detected SO with a mixing ratio in the range from 0.02 to 1 ppmv. The combination of SO and SO_2 vertical profiles forms an X-like shape indicating active photochemical inter-connection between the both gases. This upper layer was not predicted from previous modeling, and the discussion of the present results at various meetings triggered a revision of the model, including evaporation of H_2SO_4 from droplets, and its subsequent photolysis (Zhang et al., 2010, 2012). Such model refinements could be important for geo-engineering studies suggesting a deliberate injection of SO_2 in the lower stratosphere of the Earth, in order to mitigate Global Warming by the increased back scattering of solar radiation by H_2SO_4 droplets (Crutzen, 2006).

(2) At the cloud top layer (68–70 km) the mixing ratio of SO_2 decreases from the equator (0.2–0.5 ppmv) to the polar region (0.05–0.1 ppmv). The scale height of SO_2 density was calculated in the altitude range of 70–80 km: 3.5 ± 0.5 km at latitudes >50°N, and 4.1 ± 0.7 km at latitudes <50°N. No significant variation of SO_2 abundance with Venus local time was found.

(3) In the period from March 2007 to September 2008 the SO_2 mixing ratio at 70 km level was increasing from 0.05 to 0.1–0.2 ppmv. These values are compatible with previous observation at the same altitudes.

(4) An analysis of temperature dependence of SO_x abundances was performed in the upper layer, thanks to simultaneous SOIR measurements of the rotational temperature from CO_2 bands. The SO_2 mixing ratio increases with temperature from 0.1 ppmv at 165–170 K to 0.5–1 ppmv at 190–192 K. This behavior is in agreement with the possible SO_x production mechanism from gaseous H_2SO_4 photolysis at altitudes ~100 km, after evaporation from haze droplets. It confirms that the upper haze is composed of concentrated H_2SO_4 droplets.

(5) The concentration ratio $[SO_2]/[SO]$ varies between 1 and 5 at altitudes 90–100 km – a value, which is in agreement with day-side models and ground-based sub-mm observations.

Acknowledgments

Venus Express is a space mission from the European Space Agency (ESA). We wish to thank all ESA members who participated in this successful mission, and in particular H. Svedhem and D. Titov. We also thank Astrium for the design and construction of the spacecraft. We thank our collaborators at LATMOS/France, BIRA/Belgium and IKI/Russia for the design and fabrication of the instrument. We thank CNRS and CNES for funding SPICAV/SOIR in France, the Belgian Federal Science Policy Office, the European Space Agency (ESA, PRODEX program), Roscosmoc and the Russian Academy of Sciences. Oleg Korablev and Anna Fedorova acknowledge support from RFBR Grant # 10-02-93116. Denis Belyaev acknowledges support from CNES for a post-doc position at LATMOS. Xi Zhang and Yuk L. Yung were supported by NASA Grant NNX07AI63G to the California Institute of Technology.

References

Barker, E.S., 1979. Detection of SO_2 in the UV spectrum of Venus. Geophys. Res. Lett. 6, 117–120.

Belyaev, D. et al., 2008. First observations of SO_2 above Venus clouds by means of solar occultation in the infrared. J. Geophys. Res. 113, E00B25. doi:10.1029/2008JE003143.

Bertaux, J-L. et al., 2006. SPICAM on Mars Express: Observing modes and overview of UV spectrometer data and scientific results. J. Geophys. Res. 111, E10S90. doi:10.1029/2006JE002690.

Bertaux, J.-L. et al., 2007a. SPICAV on Venus Express: Three spectrometers to study the global structure and composition of the Venus atmosphere. Planet. Space Sci. 55, 1673–1700.

Bertaux, J.-L. et al., 2007b. A warm layer in Venus' cryosphere and high-altitude measurements of HF, HCl, H_2O and HDO. Nature 450, 646–649. doi:10.1038/nature05974.

Clancy, R.T., Muhleman, D.O., 1991. Long-term (1979–1990) changes in the thermal dynamical and compositional structure of the Venus mesosphere as inferred from microwave spectral observations of ^{12}CO, ^{13}CO and $C^{18}O$. Icarus 89, 129–146.

Colin, R., 1969. Spectrum of SO: Analysis of the $B^3\Sigma^- - X^3\Sigma^-$ and $A^3\Pi^- - X^3\Sigma^-$ band systems. Can. J. Phys. 47, 979–994.

Crutzen, P.J., 2006. Albedo enhancement by stratospheric sulfur injections: A contribution to resolve a policy dilemma? Clim. Change 77, 211–220.

Esposito, L.W., 1984. Sulfur dioxide: Episodic injection shows evidence for active Venus volcanism. Science 223, 1072–1074.

Esposito, L.W. et al., 1988. Sulfur dioxide at the Venus cloud tops, 1978–1986. J. Geophys. Res. 93, 5267–5276.

Esposito, L.W., Bertaux, J.-L., Krasnopolsky, V., Moroz, V.I., Zasova, L.V., 1997. Chemistry of lower atmosphere and clouds. In: Bougher, S.W., Hunten, D.M., Phillips, R.J. (Eds.), Venus, vol. II. Univ. of Arizona Press, Tucson, pp. 415–458.

Ityaksov, D., Linnartz, H., Ubachs, W., 2008. Deep-UV absorption and Rayleigh scattering of carbon dioxide. Chem. Phys. Lett. 462, 31–34.

Korablev, O.I. et al., 2004. Compact high-resolution echelle-AOTF NIR spectrometer for atmospheric measurements. In: Proc. of the 5th ICSO, ESA SP-554, held 30 March–2 April 2004 in Toulouse, France, pp. 73–80.

Krasnopolsky, V.A., 1986. In: Zahn, U.V. (Ed.), Photochemistry of the Atmosphere of Mars and Venus. Springer-Verlag, Berlin, p. 147.

Krasnopolsky, V.A., 2010. Spatially-resolved high-resolution spectroscopy of Venus. 2. Variations of HDO, OCS, and SO_2 at the cloud tops. Icarus 209, 314–322.

Krasnopolsky, V.A., 2011. Vertical profile of H_2SO_4 vapor at 70–110 km on Venus and some related problems. Icarus 215 (1), 197–203.

Lucy, L.B., 1974. An iterative technique for the rectification of observed distributions. Astron. J. 79, 745–754.

Mahieux, A. et al., 2008. In-flight performance and calibration of SPICAV SOIR onboard Venus Express. Appl. Opt. 47 (13), 2252–2265.

Mahieux, A. et al., 2010. Densities and temperatures in the Venus mesosphere and lower thermosphere retrieved from SOIR on board Venus Express: Retrieval technique. J. Geophys. Res. 115 (E12), E12014. doi:10.1029/2010JE003589.

Marcq, E. et al., 2011a. An investigation of the SO_2 content of the venusian mesosphere using SPICAV-UV in nadir mode. Icarus 211 (1), 58–69.

Marcq, E., Belyaev, D., Bertaux, J.-L., Fedorova, A., Montmessin, F., 2011b. Long-term monitoring SO_2 above the clouds of Venus using SPICAV-UV in nadir mode. EGU Gen. Assembly 13, EGU2011–EGU2603.

Markwardt, C.B., 2009. Non-linear least-squares fitting in IDL with MPFIT. In: Bohlender, D.A., Durand, D., Dowler, P. (Eds.), Astronomical Society of the Pacific Conference Series, vol. 441, pp. 251–254.

McClintock, W.E., Barth, C.A., Kohnert, R.A., 1994. Sulfur dioxide in the atmosphere of Venus. 1: Sounding rocket observations. Icarus 112, 382–388.

Mills, F.P., Esposito, L.W., Yung, Y.L., 2007. Atmospheric composition, chemistry, and clouds. In: Exploring Venus as a Terrestrial Planet, Geophysical Monograph Series, vol. 176, pp. 73–100.

Montmessin, F. et al., 2006. Stellar occultations at UV wavelengths by the SPICAM instrument: Retrieval and analysis of martian haze profiles. J. Geophys. Res. 111, E09S09. doi:10.1029/2005JE002662.

Na, C.Y., Esposito, L.W., 1995, UV observations of Venus with HST. Bull. Am. Astron. Soc. 27, 1071 (abstract).

Na, C.Y., Esposito, L.W., Skinner, T.E., 1990. International ultraviolet explorer observations of Venus SO_2 and SO. J. Geophys. Res. 95, 7485–7491.

Na, C.Y., Esposito, L.W., McClintock, W.E., Barth, C.A., 1994. Sulfur dioxide in the atmosphere of Venus. 2: Modeling results. Icarus 112, 389–395.

Nevejans, D. et al., 2006. Compact high-resolution spaceborne echelle grating spectrometer with acousto-optical tunable filter based order sorting for the infrared domain from 2.2 to 4.3 μm. Appl. Opt. 45, 5191–5206.
Parkinson, W., 2003. Absolute absorption cross section measurements of CO_2 in the wavelength region 163–200 nm and the temperature dependence. Chem. Phys. 290, 251–256.
Phillips, L.F., 1981. Absolute absorption cross sections for SO between 190 and 235 nm. J. Phys. Chem. 85, 3994–4000.
Quemerais, E. et al., 2006. Stellar occultations observed by SPICAM on Mars Express. J. Geophys. Res. 111, E09S04. doi:10.1029/2005JE002604.
Rothman, L.S. et al., 2005. The HITRAN 2004 molecular spectroscopic database. J. Quant. Spectrosc. Radiat. Transf. 96, 139–204. doi:10.1016/j.jqsrt.2004.10.008.
Royer, E., Montmessin, F., Bertaux, J.-L., 2010. NO emission as observed by SPICAV during stellar occultations. Planet. Space Sci. 58 (10), 1314–1326.
Rufus, J., Stark, G., Smith, P.L., Pickering, J.C., Thorne, A.P., 2003. High-resolution photoabsorption cross section measurements of SO_2, 2: 220–325 nm at 295 K. J. Geophys. Res. (Planets) 108, 5011–5016.
Sandor, B.J., Todd Clancy, R., Moriarty-Schieven, G., Mills, F.P., 2010. Sulfur chemistry in the Venus mesosphere from SO_2 and SO microwave spectra. Icarus 208, 49–60.
Sandor, B.J., Clancy, R.T., Moriarty-Schieven, G., 2012. Upper limits for H_2SO_4 in the mesosphere of Venus. Icarus 217 (2), 839–844.
Thuillier, G. et al., 2009. SOLAR/SOLSPEC: Scientific objectives, instrument performance and its absolute calibration using a blackbody as primary standard source. Sol. Phys. 257, 185–213.
Titov, D.V. et al., 2006. Venus Express: Scientific goals, instrumentation, and scenario of the mission. Cosmic Res. 44, 334–348.
Vandaele, A.C. et al., 2008. Composition of the Venus mesosphere measured by solar occultation at infrared on board Venus Express. J. Geophys. Res. 113, E00B23. doi:10.1029/2008JE003140.
Wu, R.C.Y. et al., 2000. Measurements of high-, room-, and low-temperature photoabsorption cross sections of SO_2 in the 2080- to 2950-Å region, with application to Io. Icarus 145, 289–296.
Yung, Y.L., Demore, W.B., 1982. Photochemistry of the stratosphere of Venus – Implications for atmospheric evolution. Icarus 51 (2), 199–247.
Zasova, L.V., Moroz, V.I., Esposito, L.W., Na, C.Y., 1993. SO_2 in the middle atmosphere of Venus: IR measurements from Venera-15 and comparison to UV data. Icarus 105, 92–109.
Zasova, L.V., Moroz, V.I., Linkin, V.M., Khatuntsev, I.V., Maiorov, B.S., 2006. Structure of venusian atmosphere from surface up to 100 km. Cosmic Res. 44 (4), 364–383.
Zhang, X. et al., 2010. Photolysis of sulphuric acid as the source of sulphur oxides in the mesosphere of Venus. Nature Geosci. 3 (12), 834–837.
Zhang, X., Liang, M.-C., Mills, F.P., Belyaev, D., Yung, Y.L., 2012. Sulfur chemistry in the middle atmosphere of Venus. Icarus 217 (2), 714–739.